Viral interference between severe acute respiratory syndrome coronavirus 2 and influenza A viruses

Shella Gilbert-Girard[1], Jocelyne Piret[1], Julie Carbonneau[1], Mathilde Hénaut[1], Nathalie Goyette[1], Guy Boivin[1*]

[1]Research Center of the CHU de Québec-Université Laval, Quebec City, QC, Canada

*Corresponding author
Email: Guy.Boivin@crchudequebec.ulaval.ca

Abstract

Some respiratory viruses can cause a viral interference through the activation of the interferon (IFN) pathway that reduces the replication of another virus. Epidemiological studies of coinfections between SARS-CoV-2 and other respiratory viruses have been hampered by non-pharmaceutical measures applied to mitigate the spread of SARS-CoV-2 during the COVID-19 pandemic. With the ease of these interventions, SARS-CoV-2 and influenza A viruses can now co-circulate. It is thus of prime importance to characterize their interactions. In this work, we investigated viral interference effects between an Omicron variant and a contemporary influenza A/H3N2 strain, in comparison with an ancestral SARS-CoV-2 strain and the 2009 pandemic influenza A/H1N1 virus. We infected nasal human airway epitheliums with SARS-CoV-2 and influenza, either simultaneously or 24 h apart. Viral load was measured by RT-qPCR and IFN-α/β/λ1/λ2 proteins were quantified by immunoassay. Expression of four interferon-stimulated genes (ISGs; OAS1/IFITM3/ISG15/MxA) was also measured by RT-droplet digital PCR. Additionally, susceptibility of each virus to IFN-α/β/λ2 recombinant proteins was determined. Our results showed that influenza A, and especially A/H3N2, interfered with both SARS-CoV-2 viruses, but that SARS-CoV-2 only interfered with A/H1N1. Consistently with these results, influenza, and particularly the A/H3N2 strain, caused a higher production of IFN proteins and expression of ISGs than SARS-CoV-2. The IFN production induced by SARS-CoV-2 was marginal and its presence during coinfections with influenza was associated with a reduced IFN response. All viruses were susceptible to exogenous IFNs, with the ancestral SARS-CoV-2 and Omicron being less susceptible to type I and type III IFNs, respectively. Thus, influenza A causes a viral interference towards SARS-CoV-2 most likely through an IFN response. The opposite is not necessarily true, and a concurrent infection with both viruses leads to a lower IFN response. Taken together, these results help us to understand how SARS-CoV-2 interacts with another major respiratory pathogen.

Author summary

During the COVID-19 pandemic, non-pharmaceutical measures were able to reduce the spread of SARS-CoV-2 and most respiratory viruses. Since the ease of these measures, SARS-CoV-2 variants and other viruses, such as influenza A, have started to co-circulate and can now infect a same host and interact with each other. These interactions can lead to attenuated or aggravated infections and can affect the timing of epidemics. Therefore, it is very important to elucidate how the new SARS-CoV-2 interacts with other viruses to better predict their implications in human health and their epidemic activity. Our work contributes to better understand these interactions using viruses that have likely co-circulated after lifting mitigation interventions, i.e., SARS-CoV-2 Omicron variant and a contemporary influenza A/H3N2 strain. We studied how each virus may affect the other virus' growth and how these interactions were associated with the innate immune response of the host. We found that a prior infection with influenza A can decrease the growth of SARS-CoV-2 while the latter reduces the innate immune response. Our results help to understand the interplay between SARS-CoV-2 and influenza A in the host and may improve mathematical models predicting epidemics.

Introduction

Different respiratory viruses can infect the same host concurrently or sequentially and may thus interact with each other. The interaction can be either positive (additive or synergistic), negative (antagonistic) or neutral. Positive/negative interactions may result in an increased/decreased host susceptibility to infection by the second virus, viral loads and duration of viral shedding. In turn, these parameters may influence the rate of viral transmission at the population level. Viral interference represents a negative interaction where an infection by a first virus inhibits the infection of a second virus through the induction of a non-specific innate immune response [1]. Upon recognition of viral components, host cells produce type I interferons (IFNs; IFN-α/β) as well as type III IFNs (IFN-λ); the latter being mainly found in epithelial cells of the gastrointestinal and respiratory tracts [2]. IFN proteins stimulate the production of additional IFN molecules and the expression of a multitude of interferon-stimulated genes (ISGs) in infected and neighbouring cells, amplifying the immune response. Many ISGs act as inhibitors of the viral replication, and ISG induction contributes to the establishment of an antiviral state within cells [3]. This may result in a refractory period during which infection of these cells by another homologous or heterologous virus is reduced. Viral interference effects have been observed between different respiratory viruses in *in vitro* and *in vivo* models [4-8]. The implication of the IFN response has been confirmed in most of these reports. Epidemiologic studies also suggested that negative interactions between viruses can affect epidemic curves at the population level [4, 9]. For instance, in 2009, a human rhinovirus (HRV) epidemic peak was associated with a delay in the spread of the pandemic A/H1N1 influenza virus in different countries [10, 11].

During the coronavirus disease 2019 (COVID-19) pandemic, caused by the severe acute respiratory syndrome coronavirus 2 (SARS-CoV-2), the detection of many seasonal respiratory viruses dramatically decreased [12, 13], with the exception of some non-enveloped viruses such as rhinoviruses and adenoviruses. This was mainly due to the implementation in most countries of non-pharmaceutical

80 interventions, including social distancing, the use of facemasks, hand sanitizing, isolation, and
81 quarantine, to reduce the transmission of SARS-CoV-2 [14-18]. This caused a disturbance in seasonal
82 epidemics and resulted in off-season resurgence of some viruses when SARS-CoV-2 mitigation measures
83 were subsequently lifted [12, 19].

84 Some studies investigated the risk of coinfections with SARS-CoV-2 and other respiratory viruses
85 at the onset of the pandemic, i.e., before implementation of non-specific measures. Stowe *et al.* observed
86 that the risk of being infected with SARS-CoV-2 was 58% lower in influenza A-positive patients [20].
87 Furthermore, Nenna *et al.* reported that an early 2021 autumnal respiratory syncytial virus epidemic
88 seemed to have been interrupted by the arrival of the new Omicron variant in the population [21].
89 However, conclusions about viral interference effects between SARS-CoV-2 and other respiratory
90 viruses were difficult to establish at that time due to limited coinfection events in the population during
91 the pandemic. This underlines the necessity for additional research work in order to better understand the
92 interactions between SARS-CoV-2 and other respiratory viruses, especially with the influenza A virus
93 (IAV), which may have a major impact on morbidity and mortality.

94 So far, studies evaluating viral interference effects between SARS-CoV-2 and other respiratory
95 viruses have focused on the ancestral D614G mutant and early variants (e.g., Alpha, Beta, Delta). For
96 instance, many investigators showed that influenza A and HRV interferes with SARS-CoV-2 [22-28].
97 However, most of these studies investigated potential viral interference events between viruses that did
98 not have much opportunity to interact with SARS-CoV-2 during the pandemic, such as influenza
99 A/H1N1pdm09-derived virus, which had nearly disappeared during SARS-CoV-2's first pandemic wave
100 in 2020 [29]. After easing the non-specific interventions in spring of 2022, a late epidemic of A/H3N2
101 virus was observed in North America while A/H1N1 circulation remained low [29]. At that time, the
102 SARS-CoV-2 Omicron variant was highly prevalent [30], and interactions between these two viruses are
103 most likely to have occurred.

104 In this paper, we investigated potential viral interference effects between clinical isolates of a
105 2022 influenza A/H3N2 strain and a contemporary SARS-CoV-2 variant, i.e., Omicron (B.A.1) using
106 nasal reconstituted human airway epitheliums (HAEs) cultured at the air-liquid interface. As our group
107 already showed the occurrence of viral interference between the ancestral SARS-CoV-2 D614G strain
108 and the influenza A/H1N1pdm09 virus in the same experimental model [22], we compared both pairs of
109 viruses to evaluate potential changes that may have arisen since the onset of pandemic. We found that a
110 first infection with A/H3N2 strongly interfered with both Omicron and the ancestral D614G SARS-CoV-
111 2 virus, while the opposite was not true. On the other hand, we observed that Omicron, and to a lesser
112 extent the ancestral virus, interfered with A/H1N1. A/H1N1 also interfered with both SARS-CoV-2
113 viruses, but not as markedly as A/H3N2. We then evaluated the primary and secondary IFN responses
114 during coinfections, as well as the susceptibility of each virus to exogenous type I and type III IFNs. Our
115 results suggest that influenza A/H3N2 interferes with SARS-CoV-2 through an important IFN response.
116 One the other hand, SARS-CoV-2 inhibits the IFN response during coinfections with IAV, which may
117 reduce its ability to cause viral interference.

118

119 # Materials and methods

120 ## Cells and viruses

121 VeroE6 cells (green monkey kidney) were purchased from the American Type Culture Collection
122 (CRL-1586; Manassas, VA, USA). VeroE6/TMPRSS2 cells were provided by the NIBSC Research
123 Reagent Repository (UK), with thanks to Dr. Makoto Takeda (University of Tokyo). ST6-Gal-I MDCK
124 (Madin-Darby Canine Kidney) cells overexpressing the α2-6 sialic acid receptor (MDCK α2-6) were
125 obtained from Dr. Y. Kawaoka (University of Wisconsin, Madison, WI, USA) [31]. VeroE6 and MDCK

126 α2-6 cells were cultured in minimum essential medium (MEM; Invitrogen, Carlsbad, CA, USA)
127 supplemented with 10% fetal bovine serum (FBS; Invitrogen) and 1% HEPES. Culture medium for
128 MDCK α2-6 also contained puromycin (7.5 µg/ml). VeroE6/TMPRSS2 were cultured in Dulbecco's
129 modified Eagle's medium (DMEM) supplemented with 10% FBS, 1% HEPES and 1 mg/ml geneticin
130 (Life Technologies, Carlsbad, CA, USA). Nasal reconstituted HAEs (MucilAir™, pool of donors,
131 EP02MP) and their culture medium were provided by Epithelix Sàrl (Geneva, Switzerland). HAEs were
132 cultured in 24-well inserts at the air-liquid interface. All cells and HAE inserts were maintained at 37°C
133 with 5% CO_2.

134 Influenza A/H3N2 virus (clade 3C.2a1b.2a.2; isolated from a clinical sample collected in April
135 2022 in Quebec City, Canada) and influenza A/California/7/2009 H1N1pdm09 virus were amplified on
136 MDCK α2-6 in MEM supplemented with 1% HEPES and 1 µg/ml trypsin treated with N-tosyl-L-
137 phenylalanine chloromethyl ketone (Sigma, Oakville, ON, Canada). Viral titers were determined by
138 plaque assays. SARS-CoV-2 strain Quebec/CHUL/21697, an ancestral strain bearing the spike
139 substitution D614G (referred to as D614G), and SARS-CoV-2 strain Quebec/CHUL/904,274 (Omicron:
140 B.1.1.529, sub-lineage BA.1.15; referred to as Omicron) were isolated from nasopharyngeal swabs
141 recovered in Quebec City, Canada, in March 2020 and December 2021, respectively. D614G was
142 amplified on VeroE6 cells in MEM supplemented with 1% HEPES. Omicron was amplified on
143 VeroE6/TMPRSS2 cells in DMEM with 1% HEPES. Viral titers were then determined by plaque assays.
144 All experimental work using infectious SARS-CoV-2 was performed in a Biosafety Level 3 (BSL3)
145 facility at the CHU de Québec-Université Laval.

146

147 **Infection kinetics in HAEs**

148 Before infection, the apical poles of HAEs were washed with 200 µl of pre-warmed Opti-MEM
149 (Gibco; ThermoFisher Scientific, Waltham, MA, USA) during 10 min at 37°C and pipetting up and down
150 a few times to remove the mucus layer. The apical poles of HAEs were infected with each single virus
151 at a multiplicity of infection (MOI) of 0.02 (considering that each HAE was made of 500 000 cells), in
152 200 µl of Opti-MEM. HAEs were incubated for 1 h at 37°C with 5% CO_2, and the inoculum was then
153 removed. For simultaneous coinfections, both viruses, at the same MOI, were added in 200 µl of medium.
154 Sequential coinfections were made with each viral infection occurring 24 h apart. The trans-epithelial
155 electrical resistance (TEER) was measured every 48 h from the first infection day, using a Millicell®
156 ERS-2 Voltohmmeter (Sigma-Aldrich, St. Louis, MO, USA). In single infections and when specified,
157 the viability of HAEs was assessed by a MTS assay (CellTiter 96® AQueous One Solution Cell
158 Proliferation Assay; Promega, Madison, WI, USA) by addition of 20 µl of MTS solution with 180 µl of
159 Opti-MEM on the apical pole of HAEs. After an incubation of 1 h in the dark at 37°C with 5% CO_2, the
160 absorbance was measured at 490 nm in a 96-well plate, using a Synergy HTX multi-mode reader (BioTek
161 Instruments, Winooski, VT, USA). Fig 1 summarizes the experimental design.

162 Each day following the first infection, the apical pole of HAEs was washed with 200 µl of pre-
163 warmed Opti-MEM by incubating for 10 min at 37°C with 5% CO_2 and then pipetting the supernatant
164 up and down. The apical wash was collected and stored at -80°C for viral RNA load determination. Every
165 48 h, the basolateral medium was taken and replaced with 500 µl of fresh pre-warmed MucilAir™ culture
166 medium. The collected basolateral medium was snap-frozen and stored at -80°C for cytokine
167 quantification. After 120 h post-infection (p.i.), HAEs were lysed for ISG quantification by RT-droplet
168 digital PCR. Uninfected HAEs were manipulated the same way as infected ones for 120 h prior to lysis.

169

170 Treatment of HAEs with recombinant IFN proteins and IFN inhibitors

171 Recombinant human IFN-β (8499-IF) and IFN-λ2 (1587-IL) were purchased from R&D Systems
172 (Minneapolis, MN, USA). Both were reconstituted in phosphate-buffered saline (PBS) with 0.1% bovine
173 serum albumin (BSA; Sigma-Aldrich) and added to the basolateral pole at a concentration of 100 ng/ml.
174 Recombinant human IFN-α2a (H6041; Sigma-Aldrich) was reconstituted in PBS with 0.1% BSA and
175 added to the basolateral pole at a final concentration of 100 U/ml. HAEs were treated 24 h before primary
176 infection and then daily in the basolateral medium until 120 h p.i.

177 Ruxolitinib (Cayman Chemical, Ann Arbor, MI, USA) was reconstituted in dimethyl sulfoxide
178 (DMSO). It was added to the basolateral pole at a concentration of 5 μM 24 h prior to infection and was
179 maintained at that concentration until 120 h p.i. BX795 (Sigma-Aldrich) was reconstituted in DMSO. It
180 was added to the basolateral pole at a concentration of 6 μM 24 h prior to infection and was maintained
181 at that concentration until 120 h p.i., as previously described in HAEs [4, 22, 23, 27].

182

183 Viral RNA load quantification by RT-qPCR

184 Apical washes (100 μl) were first incubated in lysis buffer for 1 h at room temperature to
185 inactivate SARS-CoV-2 before leaving the BSL3 facility. Viral RNA isolation was performed using the
186 MagNA Pure LC system (Total nucleic acid isolation kit, Roche Molecular System, Laval, QC, Canada)
187 or the EZ2 Connect system (EZ1&2 Virus Mini Kit v2.0, Qiagen, Toronto, ON, Canada). Then, reverse
188 transcription quantitative PCR (RT-qPCR) assays were performed with the QuantiTect Virus + ROX
189 Vial Kit (Qiagen, Toronto, ON, Canada) in a LightCycler® 480 system (Roche Molecular System), using
190 primers and probes targeting the M gene of influenza A (sequences available upon request) and the E
191 gene of SARS-CoV-2 [32]. A value corresponding to the detection limit of the assays was attributed to
192 samples with undetectable RNA levels.

193

194 IFN protein quantification by magnetic bead-based immunoassay

195 Medium samples collected at the basolateral pole of HAEs (250 µl) were thawed and inactivated
196 with 1% Triton X-100 for 1 h at room temperature before leaving the BSL3 facility. A multiplex magnetic
197 bead-based immunoassay was performed for four targets (IFN-α, IFN-β, IL-28A/IFN-λ2 and IL-29/IFN-
198 λ1) using a Bio-Plex Pro™ Human Inflammation Panel 1 Express assay (Bio-Rad Laboratories Ltd.,
199 Mississauga, ON, Canada) according to the manufacturer's instructions. Mean fluorescence intensity
200 from all the bead combinations was measured using a Bioplex 200 system and the Bioplex Manager
201 Software V6.2 (Bio-Rad Laboratories Ltd.).

202

203 ISG expression by RT-ddPCR

204 After 120 h p.i., HAEs were treated with 100 µl of lysis buffer for 1 h at room temperature to
205 inactivate SARS-CoV-2 before leaving the BSL3 facility. Viral RNA isolation was performed using the
206 MagNA Pure LC system (Total nucleic acid isolation kit, Roche Molecular System) or the EZ2 Connect
207 system (EZ1&2 Virus Mini Kit v2.0, Qiagen). Then, one-step reverse transcription droplet digital PCR
208 (RT-ddPCR) assays were performed with the One-step RT-ddPCR Advanced Kit for probes (Bio-Rad
209 Laboratories Ltd.), using primers and probes targeting 2',5'-oligoadenylate synthetase 1 (OAS1),
210 interferon-induced transmembrane protein 3 (IFITM3), interferon-stimulated gene 15 (ISG15), and
211 myxovirus resistance protein A (MxA). Primers and probes are described in S1 Table. Expression of the
212 ISGs was compared to that of a housekeeping gene (18S). For this latter gene, reverse transcription was
213 done separately using the SuperScript™ IV First-Strand Synthesis System (Invitrogen™, ThermoFisher
214 Scientific) according to the manufacturer's instructions using 5 µl of RNA. The ddPCR reaction was

215 performed using QX200™ ddPCR™ EvaGreen SuperMix (Bio-Rad Laboratories Ltd.). For all ddPCR
216 experiments, droplets were generated using a QX200™ Droplet Generator (Bio-Rad Laboratories Ltd.)
217 and PCR reactions were performed using a C1000 Touch Thermal cycler (Bio-Rad). Acquisition was
218 made with a QX200™ Droplet Reader (Bio-Rad Laboratories Ltd.), with the software QX Manager 1.2.

219

220 Statistical analysis

221 Statistical analyses were performed with GraphPad Prism version 9.4.0 (GraphPad Software, La
222 Jolla, CA, USA). A one-way Brown-Forsythe and Welch analysis of variance (ANOVA) test with
223 posthoc Dunnett's T3 multiple comparisons test was used to compare viral RNA loads, ISG mRNAs or
224 IFN protein levels in the different experimental conditions.

225 Results

226 Interference between SARS-CoV-2 and IAV

227 We first investigated the interactions between the contemporary SARS-CoV-2 Omicron variant
228 and the influenza A/H3N2 strain that were circulating after the ease of non-pharmacological
229 interventions. Reconstituted HAEs were infected with each single virus or coinfected with the two viruses
230 simultaneously or sequentially (24 h apart). Fig 2A shows that a prior infection of HAEs with A/H3N2
231 greatly reduced the replication of Omicron by 3 logs compared to Omicron alone at 96 h p.i. However,
232 when HAEs were infected with Omicron first or simultaneously to A/H3N2, the replication of Omicron
233 was similar to that of the single infection. Fig 2B shows that in all A/H3N2 and Omicron coinfections
234 (either simultaneous or sequential), the growth of A/H3N2 was comparable to that of the single virus.
235 Thus, although A/H3N2 interferes with Omicron when added 24 h earlier, the opposite is not true. When

236 investigating the interactions between the SARS-CoV-2 and the IAV subtype circulating at the onset of
237 the pandemic (i.e., in winter 2020), our group previously showed that ancestral D614G interfered with
238 influenza A/H1N1pdm09 virus [22]. We thus evaluated whether, in contrast to Omicron, SARS-CoV-2
239 D614G would interfere with an A/H3N2 strain from 2022 in HAEs (Fig 2C-D). With this strain as well,
240 we observed that A/H3N2 causes viral interference towards SARS-CoV-2, but not the opposite.

241 We next tested coinfections between the two SARS-CoV-2 strains and A/H1N1. When A/H1N1
242 was the primary virus, the growth of Omicron was reduced by over 1 log throughout the infection (Fig
243 3A). However, in contrast to A/H3N2, in HAEs infected with Omicron first, the growth of A/H1N1 was
244 inhibited (Fig 3B). Interestingly, in HAEs infected with A/H1N1 prior to Omicron, A/H1N1 seemed to
245 grow faster than in other conditions. In sequential A/H1N1 and D614G coinfections (Fig 3C-D), A/H1N1
246 caused more interference than with Omicron since the viral load of D614G barely increased and was
247 reduced by 2 logs at 96 h p.i., compared to D614G alone. The simultaneous coinfection of D614G and
248 A/H1N1 also resulted in inhibition of SARS-CoV-2 throughout the infection, albeit not significantly. On
249 the other hand, a 1-log reduction of A/H1N1 was observed from 48 h to 96 h p.i. when HAEs were
250 infected with D614G first, although this was not statistically significant.

251 Of note, all viruses caused a reduction of the TEER of HAEs, especially A/H3N2 (panel A in S1
252 Fig). We thus verified the cellular viability of HAEs during single infections with each virus by MTS
253 assays and concluded that all HAEs survived the infection (panel B in S1 Fig). Additionally, we measured
254 the expression of a housekeeping gene (18S) at 120 h p.i. in lysates of infected HAEs and confirmed that
255 cells still adhered to the insert membranes at the end of the kinetics experiment with all viruses (panel C
256 in S1 Fig). Taken together, these results confirmed that HAEs infected with A/H3N2, albeit showing a
257 higher reduction of the TEER than those infected with the other viruses, did survive until the end of the
258 experiments. Thus, our results suggest that a primary infection with IAV interferes with SARS-CoV-2

259 D614G, and that the interference induced by A/H3N2 was more important than that of A/H1N1.
260 However, SARS-CoV-2 Omicron, and to a lesser extent D614G, interfere only with A/H1N1.

261

262 SARS-CoV-2 induces a weaker IFN response than IAV and inhibits IFN 263 production in coinfections

264 To better understand the role of IFN in the viral interference process between IAV and SARS-
265 CoV-2, we first investigated the production of type I and type III IFNs induced by viruses in single
266 infections and coinfections. The basolateral medium of infected HAEs was collected every 48 h and the
267 levels of IFN proteins (IFN-α/β/λ1/λ2) were measured by magnetic bead-based immunoassay. No IFN-
268 α protein was detected in any condition, as reported elsewhere [25, 33]. At 24 h p.i., there was no IFN-β
269 detected, and the production of IFN-λ1 and λ2 was minimal and not significantly different for all infection
270 conditions tested (S2 Fig). IAV, especially A/H3N2, caused a much greater secretion of type I and type
271 III IFN proteins than SARS-CoV-2, with maximal values reached at 72 h and 120 h p.i. for A/H3N2 and
272 A/H1N1, respectively (Fig 4). Levels of type III IFNs, especially IFN-λ2, were much higher than those
273 of IFN-β. Single infections with both SARS-CoV-2 viruses induced no IFN-β and only a marginal IFN-
274 λ1 and λ2 production. Interestingly, IFN secretion was decreased in almost all coinfections with IAV
275 compared to IAV alone, especially when SARS-CoV-2 was added first or simultaneously. This effect
276 may result from the mechanisms of immune evasion induced by SARS-CoV-2 to escape or reduce IFN
277 response [34, 35]. However, at 72 h p.i., levels of IFNs were more elevated in the sequential A/H1N1 –
278 Omicron coinfection than with A/H1N1 in single infection or in other coinfection conditions (Fig 4G-H-
279 I). We observed that A/H1N1 grew more quickly when it is added before Omicron (Fig 3), which may
280 have led to a faster IFN response. Overall, the higher production of type I and type III IFNs induced by

281 IAV, especially A/H3N2, could explain why it interferes more readily with SARS-CoV-2 compared to
282 A/H1N1.

283

284 SARS-CoV-2 induces a weaker ISG expression than influenza A

285 Type I and type III IFNs are associated with the expression of several ISGs [2]. We thus
286 investigated the expression of four ISGs acting on different steps of viral infection (i.e., OAS1, IFITM3,
287 ISG15, MxA) in lysates of HAEs infected with A/H3N2, A/H1N1, D614G and Omicron viruses in single
288 and coinfections. Uninfected HAEs exhibited a minimal ISG expression (panel A in S3 Fig) that was
289 significantly lower than those of all infected HAEs ($p \leq 0.05$). The expression of the different ISGs was
290 almost similar between single infections with the two SARS-CoV-2 strains as well as between single
291 infections with the two influenza A viruses (S3 Fig).

292 Fig 5 shows that SARS-CoV-2 (Omicron and D614G) induced a significantly lower expression
293 ($p \leq 0.05$) of the different ISGs than influenza A/H1N1 and A/H3N2. In all SARS-CoV-2 and A/H3N2
294 coinfections, the ISG expression was almost comparable to that of SARS-CoV-2 alone, regardless of the
295 first infecting virus. In Omicron and A/H1N1 coinfections, all four ISGs were more inhibited when
296 Omicron was the first virus. In the simultaneous coinfection or when A/H1N1 was the primary virus,
297 expression of the ISGs was more often intermediate between that of Omicron and A/H1N1. In contrast,
298 in D614G and A/H1N1 coinfections, the expression of almost all ISGs was more or less similar to that
299 induced by A/H1N1 alone. These results thus partly reflect what was observed with the primary IFN
300 response, with a stronger immune response being induced by IAV than by SARS-CoV-2.

301

302 SARS-CoV-2 and IAV have similar susceptibility to type I and III IFNs

303 The susceptibility of different viruses to the IFN response is another factor that could affect viral
304 interference effects [1]. We thus assessed the susceptibility of SARS-CoV-2 and IAV to exogenous type
305 I and III IFNs by treating infected HAEs with recombinant IFN-α2a, -β and -λ2 proteins (Fig 6). The
306 viral RNA load of SARS-CoV-2 Omicron was markedly decreased by 3 to 4 logs at 120 h p.i. in the
307 presence of IFN-α and β. Treatment with type III IFN was much less effective, causing a 1-log reduction
308 of the viral RNA load of Omicron early in the infection. The viral RNA load of Omicron eventually
309 reached the same level as that of untreated controls later during the infection. D614G was slightly less
310 susceptible than Omicron to IFN-α and β (difference not significant at most time points), with a reduction
311 of its growth slightly lower than 3 logs, but it was a little more susceptible to IFN-λ2 (2-log reduction)
312 at 120 h p.i. Both A/H3N2 and A/H1N1 were more susceptible to type I IFNs than SARS-CoV-2
313 (especially D614G), with about 4-log of reduction at 120 h p.i. There was no significant difference
314 between the two IAVs but A/H3N2 was slightly less affected by IFN-λ2, with only 1-log reduction, while
315 the growth of A/H1N1 was inhibited by 2 logs throughout the infection. Thus, the viral interference
316 between SARS-CoV-2 and influenza does not appear to be related to a difference in their susceptibility
317 to IFN.

318

319 Effects of an IFN inhibitor on viral replication and interference

320 Finally, we investigated whether viral interference would still occur in the presence of an IFN
321 inhibitor. We used ruxolitinib, a JAK1-JAK2 inhibitor that has been approved for the treatment of
322 multiple diseases, such as myelofibrosis, osteofibrosis, polycythemia vera, and steroid-refractory acute
323 graft-*versus*-host disease. We first treated HAEs with ruxolitinib before and during single infections to
324 evaluate its effects on the viral growth of IAV and SARS-CoV-2 (Fig 7). As expected, ruxolitinib
325 increased the viral RNA loads of D614G and A/H1N1 by up to 1.5 and 2 logs, respectively. In contrast,

326 the replication of Omicron and A/H3N2 remained mostly unaffected. We next looked at the effect of
327 ruxolitinib on the viral interference between influenza and SARS-CoV-2 Omicron. However, we found
328 that the growth of Omicron in coinfection with both IAV was still reduced in the presence of ruxolitinib
329 (Fig 7C-D). Indeed, a prior A/H3N2 infection reduced by more than 3 logs the viral RNA load of
330 Omicron in presence (Fig 7) or absence (Fig 2) of ruxolitinib, whereas a primary A/H1N1 infection
331 decreased the viral RNA load of Omicron by 2.5 logs and 1.5 logs with (Fig 7) and without (Fig 3)
332 ruxolitinib, respectively. Thus, the IFN inhibitor did not rescue the replication of Omicron during
333 sequential coinfections with IAV.

334 However, we observed a marked drop of the TEER in all infected HAEs, especially when IAV
335 infections were done in the presence of ruxolitinib (panel A in S4 Fig). The viability of HAEs infected
336 with IAV and treated with ruxolitinib was also markedly decreased when assessed by MTS assays
337 (especially for A/H3N2; panel B in S4 Fig) and 18S mRNA quantification at 120 h p.i. (for both A/H1N1
338 and A/H3N2; panel C in S4 Fig). Furthermore, an almost complete loss of cells on the inserts was seen
339 at the end of the kinetics experiments. Nevertheless, we were able to confirm the inhibitory activity of
340 ruxolitinib on ISG expression in HAEs infected with SARS-CoV-2, which were still viable at 120 h p.i.
341 (panel D in S4 Fig).

342 We then evaluated the effects of another IFN inhibitor, BX795, which inhibits TANK-binding
343 kinase 1 activity, on the viral interference between A/H3N2 and Omicron (S5 Fig). We also observed
344 that the IFN inhibitor did not rescue the growth of Omicron and resulted in an even larger difference in
345 viral RNA loads (almost 4 logs) compared to that of Omicron alone. With BX795 as well, infection with
346 A/H3N2 resulted in a highly increased cell death rate, as indicated by TEER measurements and MTS
347 assays (panels B-C in S5 Fig). Overall, our results suggest that a rescue of Omicron replication could not
348 be seen due to the increased cell death in HAEs infected with IAV in the presence of both IFN inhibitors.

349

350 # Discussion

351 The COVID-19 pandemic has dramatically affected the circulation of seasonal viruses, mainly as
352 a result of the introduction of non-pharmaceutical interventions to mitigate the spread of SARS-CoV-2.
353 Nevertheless, viral interference events have been reported between SARS-CoV-2 and other respiratory
354 viruses [20, 21]. Previous studies using human respiratory epitheliums have already shown viral
355 interference effects between the ancestral SARS-CoV-2 (D614G) and influenza A/H1N1pdm09 (the
356 subtype that circulated at the onset of the COVID-19 pandemic) [22, 24, 25, 36]. In this paper, we further
357 explored events that have likely happened after lifting non-pharmacological measures by investigating
358 the interactions between contemporary SARS-CoV-2 Omicron and IAV H3N2 (clade 3C.2a1b.2a.2)
359 viruses. We also compared both pairs of viruses to evaluate whether potential changes in their interactions
360 may have occurred over time. To better understand the role played by IFN in the viral interference effects,
361 we looked at the primary and secondary IFN responses induced by each virus, as well as their
362 susceptibility to type I and type III IFN proteins.

363 We found that both influenza A/H1N1 and A/H3N2 reduced the replication of SARS-CoV-2
364 D614G in a similar manner whereas A/H3N2 caused more interference with Omicron than A/H1N1. The
365 two SARS-CoV-2 strains, and mainly Omicron, also interfered with A/H1N1, but not with A/H3N2. The
366 main IFN proteins induced by IAV and SARS-CoV-2 infections were IFN-λ1 and λ2, which is in
367 accordance with previous reports showing that type III IFNs are the first and predominant antiviral
368 response in airway epitheliums [2, 37]. In agreement with previous reports [23, 25, 27, 33, 36], we
369 observed that IAV strains caused a more important IFN-β and IFN-λ release in HAEs compared to SARS-
370 CoV-2 strains. Among the two influenza strains, A/H3N2 induced the strongest IFN production. As the
371 IFN response, the ISG expression was also higher during IAV infections than with SARS-CoV-2. All

372 viruses were more susceptible to type I than to type III exogenous IFNs. Compared to Omicron, we
373 observed that D614G exhibits a slightly lower susceptibility to IFN-I and a slightly higher susceptibility
374 to IFN-λ2. These results partly differ from previous works showing that more recent SARS-CoV-2
375 variants were less susceptible than earlier strains to type III and type I IFNs [38, 39]. Differences in
376 strains and cells used could account for this discrepancy.

377 During coinfections with A/H3N2, we observed that a first infection with the influenza virus
378 strongly reduced the replication of both SARS-CoV-2 D614G and Omicron, while SARS-CoV-2 did not
379 interfere with A/H3N2. Another study, using bronchial HAEs, showed that A/H3N2 interfered with
380 SARS-CoV-2 Beta variant, but it was not affected by SARS-CoV-2 [23]. This is consistent with A/H3N2
381 inducing strong primary and secondary IFN responses, which can inhibit subsequent infection by another
382 virus. In contrast, an infection with SARS-CoV-2, which does not lead to a strong activation of the IFN
383 response, is less likely to cause viral interference. In this context, SARS-CoV-2 only induced the
384 production of low amounts of type III IFN and A/H3N2 was not very susceptible to IFN-λ. Furthermore,
385 it is well known that many proteins of SARS-CoV-2 can inhibit the primary and secondary IFN responses
386 by targeting various components of the signaling pathways [34, 35, 40-44]. During our coinfection
387 studies with A/H3N2, the mechanisms of immune evasion of SARS-CoV-2 seemed to have inhibited the
388 IFN response, especially when SARS-CoV-2 was the primary virus or during simultaneous coinfections.
389 Expression of all four ISGs (OAS1, IFITM3, ISG15, MxA) was also reduced in all coinfections with
390 SARS-CoV-2 (either D614G or Omicron) and A/H3N2, compared to that of A/H3N2 alone. Regardless
391 of which virus was infecting first, SARS-CoV-2 reduced ISG expression to levels similar to those
392 induced by SARS-CoV-2 alone. Another factor that could be at play in the viral interference observed is
393 that SARS-CoV-2 has a slower growth rate than IAV, which makes it more susceptible to interactions
394 with faster growing viruses [45]. Furthermore, as A/H3N2 causes more damage to the HAEs than SARS-

395 CoV-2, as reported by others [23], the number of host cells available for SARS-CoV-2 infection may be
396 reduced, which may contribute to the interfering effect induced by A/H3N2.

397 We also confirmed results of previous reports showing that A/H1N1pdm09 interfered with
398 ancestral SARS-CoV-2 in human respiratory epitheliums [22, 24, 25, 36] and extended these data to the
399 Omicron variant. We observed that A/H1N1 did not interfere as strongly with Omicron as A/H3N2. This
400 could be partly related to the weaker IFN response induced by A/H1N1 compared to A/H3N2. Based on
401 our kinetics experiments, the growth rate of A/H1N1 was also slightly slower than that of A/H3N2
402 suggesting that A/H1N1 may have a lower ability to interfere with other viruses [45]. Furthermore,
403 Omicron might have developed more effective mechanisms to evade the low IFN response caused by
404 A/H1N1 than D614G, as suggested in some reports [38, 39, 46, 47]. Compared to D614G, Omicron was
405 slightly more sensitive to IFN-α and -β but it was less sensitive to IFN-λ2, which was mainly expressed
406 during IAV infection. Although IFN production was almost similar in coinfections with A/H1N1 and
407 both SARS-CoV-2 viruses, ISG expression seemed to be higher during coinfections with D614G than
408 with Omicron. This could also explain the stronger interference of A/H1N1 towards D614G compared
409 to Omicron. Contrarily to what was observed with A/H3N2, SARS-CoV-2 Omicron interfered with
410 A/H1N1. D614G showed a tendency to interfere with A/H1N1 as well, but this effect was not significant.
411 We may suggest that although SARS-CoV-2 does not induce a strong IFN response, the low amount of
412 IFN-λ produced might be sufficient to affect the growth of A/H1N1, which shows a tendency to be
413 slightly more susceptible to type III IFN than A/H3N2. Nevertheless, the observation that SARS-CoV-2
414 could interfere with IAV is contradictory in several reports [22, 24-26, 36]. Differences in viral strains,
415 host cells, timing of infections and study designs might explain these inconsistent results.

416 To confirm the involvement of the IFN response in viral interference effects, HAEs were
417 incubated prior and during single and coinfections with an IFN inhibitor, ruxolitinib. During single
418 infections with D614G and A/H1N1, viral RNA loads were increased in presence of ruxolitinib, as

419 previously observed by our group with another IFN inhibitor, BX795 [22]. In contrast, ruxolitinib did
420 not affect the growth of Omicron and A/H3N2. Shalamova *et al.* also observed that the growth of the
421 ancestral SARS-CoV-2, but not Omicron, was increased in presence of ruxolitinib [46]. The effects of
422 ruxolitinib and BX795 on the growth of IAV and SARS-CoV-2 reported in several papers [22, 23, 46,
423 48-50] were highly divergent; some described no significant effect whereas others showed an increased
424 IAV and SARS-CoV-2 replication. The nature of these discrepancies could be related to the experimental
425 conditions and viral strains used. Surprisingly, in our experiments, ruxolitinib and BX795 did not rescue
426 the replication of Omicron in HAEs coinfected with A/H3N2 or A/H1N1. This lack of effects was related
427 to the rapid and severe damage in HAEs infected with IAV in the presence of ruxolitinib or BX795. As
428 we observed no severe damage in HAEs infected with SARS-CoV-2, we could confirm that ruxolitinib
429 effectively inhibited the ISG expression. Although we did not evaluate the cytotoxic concentrations of
430 both inhibitors in HAEs, concentrations of at least 5 µM of ruxolitinib and 6 µM of BX795 were not
431 shown to cause any cytotoxicity in various cell lines, including human airway cells [51-56]. For instance,
432 nasal HAEs have been exposed to 10 µM of ruxolitinib [50] and 6 µM of BX795 [4, 22, 23] without any
433 cytotoxicity being noted. One possible explanation could be that combined effects between IAV infection
434 and IFN inhibition may cause increased cell death in HAEs. Thus, IFN response inhibition with
435 ruxolitinib or BX795 did not allow the rescue of Omicron during coinfections with IAV due to
436 unexpected cell death, suggesting that other ways to block the IFN response should be envisaged (for
437 instance, the use of antibodies).

438 In this paper, we compared viral interference effects between IAV and SARS-CoV-2 viruses that
439 likely interacted at the onset of the pandemic and when lifting the non-pharmaceutical interventions that
440 prevented their co-circulation. We used reconstituted human nasal epitheliums obtained from a pool of
441 donors, which is a respiratory infection model more representative of clinical infections than cultured
442 cell lines. This model allows to control the timing of infection (simultaneous or sequential) to study how

443 viruses interact with each other as well as the primary and secondary IFN responses. In our study, the
444 TEER measurement, which is generally used in experiments conducted in HAEs, did not seem to be a
445 precise indicator of cell survival. We thus used complementary tests, such as the determination of the
446 expression of a housekeeping gene (18S) and MTS assays. We suggest that combining these two assays
447 with TEER measurements could be more appropriate to evaluate cell viability when using HAEs.
448 Nonetheless, this study has some limitations as HAEs remain an incomplete model that does not account
449 for the role of immune cells and other components of the adaptive immune system. Finally, the
450 unexpected cell death observed in HAEs infected with IAV in the presence of IFN inhibitors may have
451 prevented the rescue of Omicron replication. More research using these inhibitors or other ways to block
452 the IFN response, such as antibodies, in presence of respiratory viruses will be needed to fully understand
453 these observations.

454

455 # Conclusion

456 In this paper, we showed that IAV, and especially A/H3N2, interferes with SARS-CoV-2
457 Omicron, while Omicron interferes with A/H1N1 only. These results are in agreement with a recent
458 retrospective study that showed a negative correlation between SARS-CoV-2 and influenza activity and
459 an alternating dominance between the two viruses since the arrival of the Omicron variant [57]. All four
460 viruses were shown to be sensitive to exogenous IFNs, especially to type I IFN response. Thus, the
461 interfering effect of IAV on SARS-CoV-2 is probably due to the more potent primary and secondary IFN
462 responses induced by IAV. SARS-CoV-2 demonstrated a tendency to inhibit IFN production and only
463 induced a very limited IFN response. We cannot exclude, however, that other intrinsic virus-specific
464 inhibition mechanisms could also be involved in these viral interference effects [58]. A better
465 understanding of viral interference between respiratory viruses could help to improve mathematical

466 models of viral transmission to predict epidemics and future pandemics and to make public health
467 recommendations. New non-specific therapeutic avenues based on activation of the innate immune
468 response for treatment of viral infections may also arise from this knowledge.

469

470 # Acknowledgments

471 We acknowledge the bioimaging platform of the Infectious Disease Research Centre, funded by
472 an equipment and infrastructure grant from the Canadian Foundation Innovation.

473

474 # References

475 1. Piret J, Boivin G. Viral Interference between Respiratory Viruses. Emerg Infect Dis.
476 2022;28(2):273-81. doi: 10.3201/eid2802.211727. PubMed PMID: 35075991; PubMed Central
477 PMCID: PMCPMC8798701.
478 2. Mesev EV, LeDesma RA, Ploss A. Decoding type I and III interferon signalling during viral
479 infection. Nat Microbiol. 2019;4(6):914-24. Epub 20190401. doi: 10.1038/s41564-019-0421-x.
480 PubMed PMID: 30936491; PubMed Central PMCID: PMCPMC6554024.
481 3. Schoggins JW. Interferon-stimulated genes: roles in viral pathogenesis. Curr Opin Virol. 2014;6:40-
482 6. Epub 20140405. doi: 10.1016/j.coviro.2014.03.006. PubMed PMID: 24713352; PubMed Central
483 PMCID: PMCPMC4077717.
484 4. Wu A, Mihaylova VT, Landry ML, Foxman EF. Interference between rhinovirus and influenza A
485 virus: a clinical data analysis and experimental infection study. Lancet Microbe. 2020;1(6):e254-
486 e62. Epub 20200905. doi: 10.1016/s2666-5247(20)30114-2. PubMed PMID: 33103132; PubMed
487 Central PMCID: PMCPMC7580833.

488 5. Essaidi-Laziosi M, Geiser J, Huang S, Constant S, Kaiser L, Tapparel C. Interferon-Dependent and
489 Respiratory Virus-Specific Interference in Dual Infections of Airway Epithelia. Sci Rep.
490 2020;10(1):10246. Epub 20200624. doi: 10.1038/s41598-020-66748-6. PubMed PMID: 32581261;
491 PubMed Central PMCID: PMCPMC7314816.
492 6. Geiser J, Boivin G, Huang S, Constant S, Kaiser L, Tapparel C, Essaidi-Laziosi M. RSV and HMPV
493 Infections in 3D Tissue Cultures: Mechanisms Involved in Virus-Host and Virus-Virus Interactions.
494 Viruses. 2021;13(1). Epub 20210119. doi: 10.3390/v13010139. PubMed PMID: 33478119; PubMed
495 Central PMCID: PMCPMC7835908.
496 7. Laurie KL, Guarnaccia TA, Carolan LA, Yan AW, Aban M, Petrie S, et al. Interval Between
497 Infections and Viral Hierarchy Are Determinants of Viral Interference Following Influenza Virus
498 Infection in a Ferret Model. J Infect Dis. 2015;212(11):1701-10. Epub 20150505. doi:
499 10.1093/infdis/jiv260. PubMed PMID: 25943206; PubMed Central PMCID: PMCPMC4633756.
500 8. Gonzalez AJ, Ijezie EC, Balemba OB, Miura TA. Attenuation of Influenza A Virus Disease Severity
501 by Viral Coinfection in a Mouse Model. J Virol. 2018;92(23). Epub 20181112. doi:
502 10.1128/JVI.00881-18. PubMed PMID: 30232180; PubMed Central PMCID: PMCPMC6232468.
503 9. Nickbakhsh S, Mair C, Matthews L, Reeve R, Johnson PCD, Thorburn F, et al. Virus-virus
504 interactions impact the population dynamics of influenza and the common cold. Proc Natl Acad Sci
505 U S A. 2019;116(52):27142-50. Epub 20191216. doi: 10.1073/pnas.1911083116. PubMed PMID:
506 31843887; PubMed Central PMCID: PMCPMC6936719.
507 10. Linde A, Rotzén-Ostlund M, Zweygberg-Wirgart B, Rubinova S, Brytting M. Does viral interference
508 affect spread of influenza? Euro Surveill. 2009;14(40). Epub 20091008. PubMed PMID: 19822124.
509 11. Casalegno JS, Ottmann M, Duchamp MB, Escuret V, Billaud G, Frobert E, et al. Rhinoviruses
510 delayed the circulation of the pandemic influenza A (H1N1) 2009 virus in France. Clin Microbiol

511 Infect. 2010;16(4):326-9. Epub 20100128. doi: 10.1111/j.1469-0691.2010.03167.x. PubMed PMID:
512 20121829.
513 12. Principi N, Autore G, Ramundo G, Esposito S. Epidemiology of Respiratory Infections during the
514 COVID-19 Pandemic. Viruses. 2023;15(5). Epub 20230513. doi: 10.3390/v15051160. PubMed
515 PMID: 37243246; PubMed Central PMCID: PMCPMC10224029.
516 13. Galli C, Pellegrinelli L, Bubba L, Primache V, Anselmi G, Delbue S, et al. When the COVID-19
517 Pandemic Surges during Influenza Season: Lessons Learnt from the Sentinel Laboratory-Based
518 Surveillance of Influenza-Like Illness in Lombardy during the 2019-2020 Season. Viruses.
519 2021;13(4). Epub 20210416. doi: 10.3390/v13040695. PubMed PMID: 33923819; PubMed Central
520 PMCID: PMCPMC8073979.
521 14. Lai S, Ruktanonchai NW, Zhou L, Prosper O, Luo W, Floyd JR, et al. Effect of non-pharmaceutical
522 interventions to contain COVID-19 in China. Nature. 2020;585(7825):410-3. Epub 20200504. doi:
523 10.1038/s41586-020-2293-x. PubMed PMID: 32365354; PubMed Central PMCID:
524 PMCPMC7116778.
525 15. Bo Y, Guo C, Lin C, Zeng Y, Li HB, Zhang Y, et al. Effectiveness of non-pharmaceutical
526 interventions on COVID-19 transmission in 190 countries from 23 January to 13 April 2020. Int J
527 Infect Dis. 2021;102:247-53. Epub 20201029. doi: 10.1016/j.ijid.2020.10.066. PubMed PMID:
528 33129965; PubMed Central PMCID: PMCPMC7598763.
529 16. Silubonde-Moyana TM, Draper CE, Norris SA. Effectiveness of behavioural interventions to
530 influence COVID-19 outcomes: A scoping review. Prev Med. 2023;172:107499. Epub 20230405.
531 doi: 10.1016/j.ypmed.2023.107499. PubMed PMID: 37028526; PubMed Central PMCID:
532 PMCPMC10074733.
533 17. Etemad K, Mohseni P, Shojaei S, Mousavi SA, Taherkhani S, Fallah Atatalab F, et al. Non-
534 Pharmacologic Interventions in COVID-19 Pandemic Management; a Systematic Review. Arch

535 Acad Emerg Med. 2023;11(1):e52. Epub 20230723. doi: 10.22037/aaem.v11i1.1828. PubMed
536 PMID: 37671267; PubMed Central PMCID: PMCPMC10475751.
537 18. Achangwa C, Park H, Ryu S, Lee MS. Collateral Impact of Public Health and Social Measures on
538 Respiratory Virus Activity during the COVID-19 Pandemic 2020-2021. Viruses. 2022;14(5). Epub
539 20220517. doi: 10.3390/v14051071. PubMed PMID: 35632810; PubMed Central PMCID:
540 PMCPMC9146684.
541 19. Yang MC, Su YT, Chen PH, Tsai CC, Lin TI, Wu JR. Changing patterns of infectious diseases in
542 children during the COVID-19 pandemic. Front Cell Infect Microbiol. 2023;13:1200617. Epub
543 20230629. doi: 10.3389/fcimb.2023.1200617. PubMed PMID: 37457965; PubMed Central PMCID:
544 PMCPMC10339349.
545 20. Stowe J, Tessier E, Zhao H, Guy R, Muller-Pebody B, Zambon M, et al. Interactions between SARS-
546 CoV-2 and influenza, and the impact of coinfection on disease severity: a test-negative design. Int J
547 Epidemiol. 2021;50(4):1124-33. doi: 10.1093/ije/dyab081. PubMed PMID: 33942104; PubMed
548 Central PMCID: PMCPMC8135706.
549 21. Nenna R, Matera L, Licari A, Manti S, Di Bella G, Pierangeli A, et al. An Italian Multicenter Study
550 on the Epidemiology of Respiratory Syncytial Virus During SARS-CoV-2 Pandemic in Hospitalized
551 Children. Front Pediatr. 2022;10:930281. Epub 20220714. doi: 10.3389/fped.2022.930281. PubMed
552 PMID: 35911833; PubMed Central PMCID: PMCPMC9329524.
553 22. Fage C, Hénaut M, Carbonneau J, Piret J, Boivin G. Influenza A(H1N1)pdm09 Virus but Not
554 Respiratory Syncytial Virus Interferes with SARS-CoV-2 Replication during Sequential Infections
555 in Human Nasal Epithelial Cells. Viruses. 2022;14(2). Epub 20220215. doi: 10.3390/v14020395.
556 PubMed PMID: 35215988; PubMed Central PMCID: PMCPMC8879759.
557 23. Dee K, Schultz V, Haney J, Bissett LA, Magill C, Murcia PR. Influenza A and Respiratory Syncytial
558 Virus Trigger a Cellular Response That Blocks Severe Acute Respiratory Syndrome Virus 2

559 Infection in the Respiratory Tract. J Infect Dis. 2023;227(12):1396-406. doi: 10.1093/infdis/jiac494.
560 PubMed PMID: 36550077; PubMed Central PMCID: PMCPMC10266949.
561 24. Oishi K, Horiuchi S, Minkoff JM, tenOever BR. The Host Response to Influenza A Virus Interferes
562 with SARS-CoV-2 Replication during Coinfection. J Virol. 2022;96(15):e0076522. Epub 20220712.
563 doi: 10.1128/jvi.00765-22. PubMed PMID: 35862681; PubMed Central PMCID:
564 PMCPMC9364782.
565 25. Essaidi-Laziosi M, Alvarez C, Puhach O, Sattonnet-Roche P, Torriani G, Tapparel C, et al.
566 Sequential infections with rhinovirus and influenza modulate the replicative capacity of SARS-CoV-
567 2 in the upper respiratory tract. Emerg Microbes Infect. 2022;11(1):412-23. doi:
568 10.1080/22221751.2021.2021806. PubMed PMID: 34931581; PubMed Central PMCID:
569 PMCPMC8803056.
570 26. Pizzorno A, Padey B, Dulière V, Mouton W, Oliva J, Laurent E, et al. Interactions Between Severe
571 Acute Respiratory Syndrome Coronavirus 2 Replication and Major Respiratory Viruses in Human
572 Nasal Epithelium. J Infect Dis. 2022;226(12):2095-104. doi: 10.1093/infdis/jiac357. PubMed
573 PMID: 36031537; PubMed Central PMCID: PMCPMC9452145.
574 27. Dee K, Goldfarb DM, Haney J, Amat JAR, Herder V, Stewart M, et al. Human Rhinovirus Infection
575 Blocks Severe Acute Respiratory Syndrome Coronavirus 2 Replication Within the Respiratory
576 Epithelium: Implications for COVID-19 Epidemiology. J Infect Dis. 2021;224(1):31-8. doi:
577 10.1093/infdis/jiab147. PubMed PMID: 33754149; PubMed Central PMCID: PMCPMC8083659.
578 28. Cheemarla NR, Watkins TA, Mihaylova VT, Foxman EF. Viral interference during influenza A-
579 SARS-CoV-2 coinfection of the human airway epithelium and reversal by oseltamivir. J Infect Dis.
580 2023. Epub 20230918. doi: 10.1093/infdis/jiad402. PubMed PMID: 37722683.

581 29. Chow EJ, Uyeki TM, Chu HY. The effects of the COVID-19 pandemic on community respiratory
582 virus activity. Nat Rev Microbiol. 2023;21(3):195-210. Epub 20221017. doi: 10.1038/s41579-022-
583 00807-9. PubMed PMID: 36253478; PubMed Central PMCID: PMCPMC9574826.
584 30. European Centre for Disease Prevention and Control. Data on 14-day notification rate of new
585 COVID-19 cases and deaths. 2022 [cited 2023 November 7]. Available from:
586 https://www.ecdc.europa.eu/en/publications-data/data-national-14-day-notification-rate-covid-19.
587 31. Hatakeyama S, Sakai-Tagawa Y, Kiso M, Goto H, Kawakami C, Mitamura K, et al. Enhanced
588 expression of an alpha2,6-linked sialic acid on MDCK cells improves isolation of human influenza
589 viruses and evaluation of their sensitivity to a neuraminidase inhibitor. J Clin Microbiol.
590 2005;43(8):4139-46. doi: 10.1128/jcm.43.8.4139-4146.2005. PubMed PMID: 16081961; PubMed
591 Central PMCID: PMCPMC1233980.
592 32. Corman VM, Landt O, Kaiser M, Molenkamp R, Meijer A, Chu DK, et al. Detection of 2019 novel
593 coronavirus (2019-nCoV) by real-time RT-PCR. Euro Surveill. 2020;25(3). doi: 10.2807/1560-
594 7917.es.2020.25.3.2000045. PubMed PMID: 31992387; PubMed Central PMCID:
595 PMCPMC6988269.
596 33. Vanderheiden A, Ralfs P, Chirkova T, Upadhyay AA, Zimmerman MG, Bedoya S, et al. Type I and
597 Type III Interferons Restrict SARS-CoV-2 Infection of Human Airway Epithelial Cultures. J Virol.
598 2020;94(19). Epub 20200915. doi: 10.1128/jvi.00985-20. PubMed PMID: 32699094; PubMed
599 Central PMCID: PMCPMC7495371.
600 34. Hoang HD, Naeli P, Alain T, Jafarnejad SM. Mechanisms of impairment of interferon production
601 by SARS-CoV-2. Biochem Soc Trans. 2023;51(3):1047-56. doi: 10.1042/bst20221037. PubMed
602 PMID: 37199495; PubMed Central PMCID: PMCPMC10317165.

603 35. Minkoff JM, tenOever B. Innate immune evasion strategies of SARS-CoV-2. Nat Rev Microbiol.
604 2023;21(3):178-94. Epub 20230111. doi: 10.1038/s41579-022-00839-1. PubMed PMID: 36631691;
605 PubMed Central PMCID: PMCPMC9838430.
606 36. Cheemarla NR, Mihaylova VT, Watkins TA, Foxman EF. Counterintuitive effect of antiviral therapy
607 on influenza A-SARS-CoV-2 coinfection due to viral interference. bioRxiv. 2023. Epub 20230208.
608 doi: 10.1101/2023.02.07.527372. PubMed PMID: 36798412; PubMed Central PMCID:
609 PMCPMC9934525.
610 37. Galani IE, Triantafyllia V, Eleminiadou EE, Koltsida O, Stavropoulos A, Manioudaki M, et al.
611 Interferon-λ Mediates Non-redundant Front-Line Antiviral Protection against Influenza Virus
612 Infection without Compromising Host Fitness. Immunity. 2017;46(5):875-90.e6. doi:
613 10.1016/j.immuni.2017.04.025. PubMed PMID: 28514692.
614 38. Nchioua R, Schundner A, Klute S, Koepke L, Hirschenberger M, Noettger S, et al. Reduced
615 replication but increased interferon resistance of SARS-CoV-2 Omicron BA.1. Life Sci Alliance.
616 2023;6(6). Epub 20230328. doi: 10.26508/lsa.202201745. PubMed PMID: 36977594; PubMed
617 Central PMCID: PMCPMC10053418.
618 39. Guo K, Barrett BS, Morrison JH, Mickens KL, Vladar EK, Hasenkrug KJ, et al. Interferon resistance
619 of emerging SARS-CoV-2 variants. Proc Natl Acad Sci U S A. 2022;119(32):e2203760119. Epub
620 20220722. doi: 10.1073/pnas.2203760119. PubMed PMID: 35867811; PubMed Central PMCID:
621 PMCPMC9371743.
622 40. Lei X, Dong X, Ma R, Wang W, Xiao X, Tian Z, et al. Activation and evasion of type I interferon
623 responses by SARS-CoV-2. Nat Commun. 2020;11(1):3810. Epub 20200730. doi: 10.1038/s41467-
624 020-17665-9. PubMed PMID: 32733001; PubMed Central PMCID: PMCPMC7392898.
625 41. Li JY, Liao CH, Wang Q, Tan YJ, Luo R, Qiu Y, Ge XY. The ORF6, ORF8 and nucleocapsid
626 proteins of SARS-CoV-2 inhibit type I interferon signaling pathway. Virus Res. 2020;286:198074.

627 Epub 20200623. doi: 10.1016/j.virusres.2020.198074. PubMed PMID: 32589897; PubMed Central
628 PMCID: PMCPMC7309931.
629 42. Chen DY, Khan N, Close BJ, Goel RK, Blum B, Tavares AH, et al. SARS-CoV-2 Disrupts Proximal
630 Elements in the JAK-STAT Pathway. J Virol. 2021;95(19):e0086221. Epub 20210909. doi:
631 10.1128/jvi.00862-21. PubMed PMID: 34260266; PubMed Central PMCID: PMCPMC8428404.
632 43. Han L, Zhuang MW, Deng J, Zheng Y, Zhang J, Nan ML, et al. SARS-CoV-2 ORF9b antagonizes
633 type I and III interferons by targeting multiple components of the RIG-I/MDA-5-MAVS, TLR3-
634 TRIF, and cGAS-STING signaling pathways. J Med Virol. 2021;93(9):5376-89. Epub 20210509.
635 doi: 10.1002/jmv.27050. PubMed PMID: 33913550; PubMed Central PMCID: PMCPMC8242602.
636 44. Znaidia M, Demeret C, van der Werf S, Komarova AV. Characterization of SARS-CoV-2 Evasion:
637 Interferon Pathway and Therapeutic Options. Viruses. 2022;14(6). Epub 20220608. doi:
638 10.3390/v14061247. PubMed PMID: 35746718; PubMed Central PMCID: PMCPMC9231409.
639 45. Pinky L, Dobrovolny HM. SARS-CoV-2 coinfections: Could influenza and the common cold be
640 beneficial? J Med Virol. 2020;92(11):2623-30. Epub 20200619. doi: 10.1002/jmv.26098. PubMed
641 PMID: 32557776; PubMed Central PMCID: PMCPMC7300957.
642 46. Shalamova L, Felgenhauer U, Wilhelm J, Schaubmar AR, Büttner K, Schoen A, et al. Omicron
643 variant of SARS-CoV-2 exhibits an increased resilience to the antiviral type I interferon response.
644 PNAS Nexus. 2022;1(2):pgac067. Epub 20220523. doi: 10.1093/pnasnexus/pgac067. PubMed
645 PMID: 36713328; PubMed Central PMCID: PMCPMC9802332.
646 47. Sacchi A, Giannessi F, Sabatini A, Percario ZA, Affabris E. SARS-CoV-2 Evasion of the Interferon
647 System: Can We Restore Its Effectiveness? Int J Mol Sci. 2023;24(11). Epub 20230527. doi:
648 10.3390/ijms24119353. PubMed PMID: 37298304; PubMed Central PMCID: PMCPMC10253747.
649 48. Felgenhauer U, Schoen A, Gad HH, Hartmann R, Schaubmar AR, Failing K, et al. Inhibition of
650 SARS-CoV-2 by type I and type III interferons. J Biol Chem. 2020;295(41):13958-64. Epub

651 20200625. doi: 10.1074/jbc.AC120.013788. PubMed PMID: 32587093; PubMed Central PMCID:
652 PMCPMC7549028.
653 49. Yan B, Freiwald T, Chauss D, Wang L, West E, Mirabelli C, et al. SARS-CoV-2 drives JAK1/2-
654 dependent local complement hyperactivation. Sci Immunol. 2021;6(58). doi:
655 10.1126/sciimmunol.abg0833. PubMed PMID: 33827897; PubMed Central PMCID:
656 PMCPMC8139422.
657 50. Otter CJ, Bracci N, Parenti NA, Ye C, Tan LH, Asthana A, et al. SARS-CoV-2 nsp15
658 endoribonuclease antagonizes dsRNA-induced antiviral signaling. bioRxiv. 2023. Epub 20231115.
659 doi: 10.1101/2023.11.15.566945. PubMed PMID: 38014074; PubMed Central PMCID:
660 PMCPMC10680701.
661 51. Sada M, Watanabe M, Inui T, Nakamoto K, Hirata A, Nakamura M, et al. Ruxolitinib inhibits
662 poly(I:C) and type 2 cytokines-induced CCL5 production in bronchial epithelial cells: A potential
663 therapeutic agent for severe eosinophilic asthma. Immun Inflamm Dis. 2021;9(2):363-73. Epub
664 20210203. doi: 10.1002/iid3.397. PubMed PMID: 33534941; PubMed Central PMCID:
665 PMCPMC8127547.
666 52. Lee HK, Jung O, Hennighausen L. JAK inhibitors dampen activation of interferon-stimulated
667 transcription of ACE2 isoforms in human airway epithelial cells. Commun Biol. 2021;4(1):654.
668 Epub 20210602. doi: 10.1038/s42003-021-02167-1. PubMed PMID: 34079039; PubMed Central
669 PMCID: PMCPMC8172581.
670 53. Loevenich S, Spahn AS, Rian K, Boyartchuk V, Anthonsen MW. Human Metapneumovirus Induces
671 IRF1 via TANK-Binding Kinase 1 and Type I IFN. Front Immunol. 2021;12:563336. Epub
672 20210624. doi: 10.3389/fimmu.2021.563336. PubMed PMID: 34248923; PubMed Central PMCID:
673 PMCPMC8264192.

674 54. Barua S, Kaltenboeck B, Juan YC, Bird RC, Wang C. Comparative Evaluation of GS-441524,
675 Teriflunomide, Ruxolitinib, Molnupiravir, Ritonavir, and Nirmatrelvir for In Vitro Antiviral Activity
676 against Feline Infectious Peritonitis Virus. Vet Sci. 2023;10(8). Epub 20230809. doi:
677 10.3390/vetsci10080513. PubMed PMID: 37624300; PubMed Central PMCID:
678 PMCPMC10459838.
679 55. Su AR, Qiu M, Li YL, Xu WT, Song SW, Wang XH, et al. BX-795 inhibits HSV-1 and HSV-2
680 replication by blocking the JNK/p38 pathways without interfering with PDK1 activity in host cells.
681 Acta Pharmacol Sin. 2017;38(3):402-14. Epub 20170123. doi: 10.1038/aps.2016.160. PubMed
682 PMID: 28112176; PubMed Central PMCID: PMCPMC5342671.
683 56. Jaishankar D, Yakoub AM, Yadavalli T, Agelidis A, Thakkar N, Hadigal S, et al. An off-target effect
684 of BX795 blocks herpes simplex virus type 1 infection of the eye. Sci Transl Med. 2018;10(428).
685 doi: 10.1126/scitranslmed.aan5861. PubMed PMID: 29444978; PubMed Central PMCID:
686 PMCPMC7540910.
687 57. Wang Q, Jia M, Jiang M, Liu W, Yang J, Dai P, et al. Seesaw Effect Between COVID-19 and
688 Influenza From 2020 to 2023 in World Health Organization Regions: Correlation Analysis. JMIR
689 Public Health Surveill. 2023;9:e44970. Epub 20230612. doi: 10.2196/44970. PubMed PMID:
690 37191650; PubMed Central PMCID: PMCPMC10263104.
691 58. DaPalma T, Doonan BP, Trager NM, Kasman LM. A systematic approach to virus-virus
692 interactions. Virus Res. 2010;149(1):1-9. Epub 20100120. doi: 10.1016/j.virusres.2010.01.002.
693 PubMed PMID: 20093154; PubMed Central PMCID: PMCPMC7172858.
694

695 # Supporting information captions

696

697 **S1 Table. Sequences of primers and probes used for quantification of interferon-stimulated genes**
698 **and a housekeeping gene by ddPCR.**

699

700 **S1 Fig. Viability of nasal human airway epitheliums (HAEs) during single infections.**

701 A) Ratio of the trans-epithelial electrical resistance (TEER) over the starting TEER (T0 at day 0) during
702 single infection of HAEs with SARS-CoV-2 (Omicron or D614G) or influenza A (H3N2 or H1N1). B)
703 Percentage of viability over time compared to viability 24 h before infection, determined by a MTS assay.
704 Results represent the mean ± SEM of 3-6 replicates from one or two independent experiments. C) Mean
705 RNA copies per ml of 18S housekeeping gene in HAE lysates at 120 h p.i. ± SEM of 3-6 replicates from
706 one or two independent experiments.

707

708 **S2 Fig. Interferon (IFN)-λ1 and λ2 production at 24 h after single infection with SARS-CoV-2 or**
709 **IAV.**

710 Production of A) IFN-λ1 and B) IFN-λ2 proteins at the basolateral pole of nasal human airway
711 epitheliums (HAEs) after single infections with SARS-CoV-2 (Omicron or D614G) and influenza A
712 (H3N2 or H1N1), at 24 h post-infection. Non-infected HAEs are used as controls (NI). Results are
713 expressed as the mean amount in pg per ml ± SEM of 3-4 replicates from one independent experiment.

714

715 **S3 Fig. Interferon-stimulated genes (ISGs) expression of uninfected nasal human airway**
716 **epitheliums (HAEs) and during single infection with SARS-CoV-2 or IAV.**

717 A) Expression of four ISGs (OAS1, IFITM3, ISG15, MxA) in uninfected HAEs. B-D) Comparison of
718 the expression of the different ISGs in HAEs infected with SARS-CoV-2 (Omicron or D614G) or IAV

719 (H3N2 or H1N1) at 120 h p.i. Results are expressed as the mean of the ratio of ISG mRNAs over 18S
720 housekeeping gene (both in copies per μL) ± SEM, calculated using 3-6 replicates from one or two
721 independent experiments. *: $p \leq 0.05$.

722

723 **S4 Fig. Viability of nasal human airway epitheliums (HAEs) during single infection with SARS-**
724 **CoV-2 and IAV in the presence of ruxolitinib.**

725 A) Ratio of the trans-epithelial electrical resistance (TEER) over the starting TEER (T0 at day 0) and B)
726 Percentage of viability (determined by a MTS assay) over time compared to viability 24 h before
727 infection and during single infections of HAEs with SARS-CoV-2 (Omicron or D614G) or influenza A
728 (H3N2 or H1N1), in the presence of ruxolitinib (ruxo). Results represent the mean ± SEM of 3-6
729 replicates from one or two independent experiments. C) Mean of the percentage of expression of 18S
730 housekeeping gene in lysates of infected HAEs in the presence of ruxolitinib compared to the expression
731 in untreated HAEs, at 120 h p.i. ± SEM of 3-6 replicates from one or two independent experiments. D)
732 Inhibition of interferon-stimulated gene (ISG) mRNA expression by ruxolitinib in HAEs infected with
733 SARS-CoV-2. Results are expressed as the mean inhibition percentage ± SEM of 9 replicates from two
734 independent experiments.

735

736 **S5 Fig. Effect of BX795 on viral interference between Omicron and A/H3N2, and epithelium**
737 **survival.**

738 A) Viral RNA loads in nasal human airway epitheliums (HAEs) infected with SARS-CoV-2
739 Omicron alone or in sequential coinfections (seq) 24 h after A/H3N2, in the presence of BX795. Results
740 are expressed as the mean of the Log_{10} of viral RNA copies per ml ± SEM of 3 replicates from one
741 experiment. **: $p \leq 0.01$. B) Ratio of the trans-epithelial electrical resistance (TEER) over the starting

742 TEER (T0 at day 0) and C) Percentage of viability (determined by a MTS assay) over time in HAEs
743 infected with Omicron alone or sequentially with A/H3N2 and Omicron, compared to viability 24 h
744 before infection, in the presence of BX795. Results represent the mean ± SEM of 3 replicates from one
745 experiment.

746

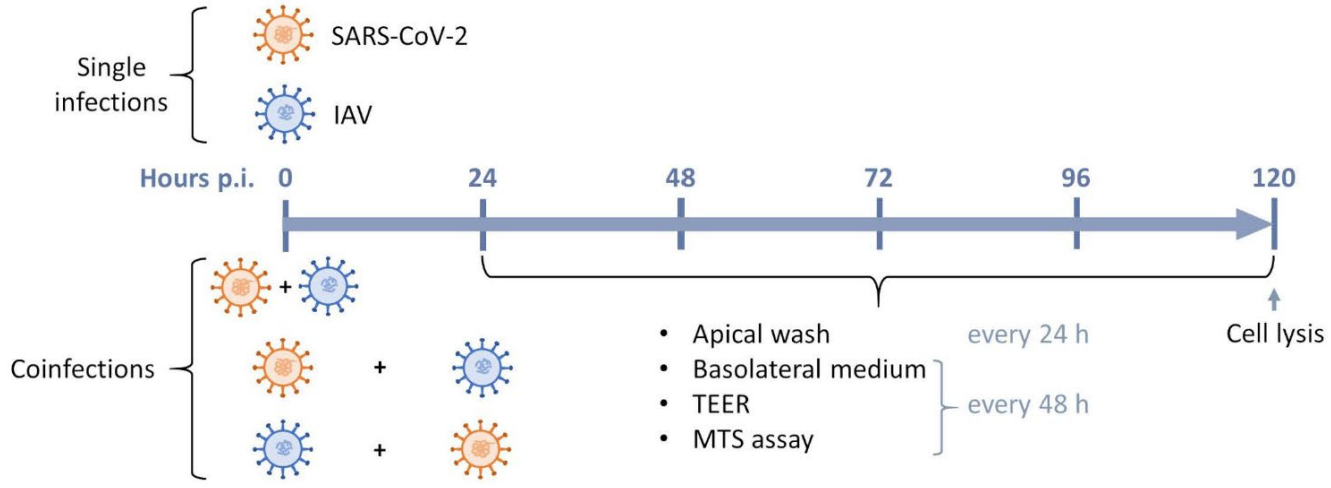

Fig 1. Timeline of SARS-CoV-2 and influenza A (IAV) single infections and coinfections in nasal human airway epitheliums (HAEs).

In coinfection experiments, SARS-CoV-2 (orange) and influenza A (blue) were added simultaneously or 24 h apart at the apical pole of HAEs. Infections were monitored for 120 h after adding the first virus. Apical washes were collected every 24 h, while basolateral medium was taken and replaced by 500 µl of fresh media every 48 h. Trans-epithelial electrical resistance (TEER) was measured every 48 h starting from the day of first infection. MTS assays were performed every 48 h starting from the day before infection. HAEs were lysed with RNA extraction buffer at 120 h post-infection (p.i.).

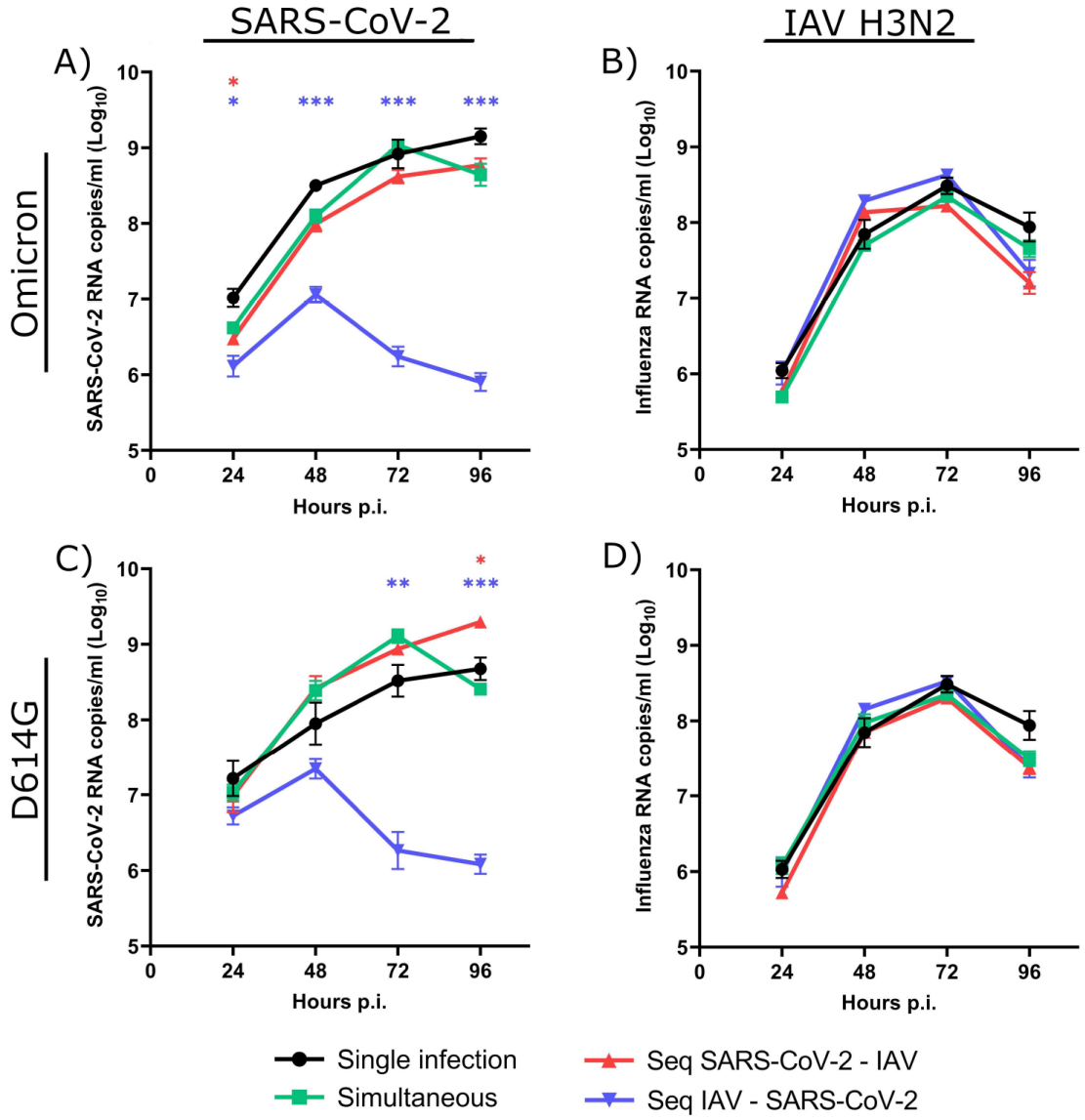

757

758 **Fig 2. Viral interference between SARS-CoV-2 strains and influenza A/H3N2.**

759 Viral RNA loads of SARS-CoV-2 (Omicron variant (A) or D614G mutant (C)) and influenza A/H3N2
760 (B, D) during single infections or simultaneous and sequential (seq) coinfections in nasal human airway
761 epitheliums (HAEs). Hours post-infection (p.i.) represent the time after the infection with either SARS-
762 CoV-2 (A, C) or influenza (B, D). Results are expressed as the mean of the Log_{10} of viral RNA copies
763 per ml ± SEM of 3-4 replicates of HAEs in one experiment. *: $p \leq 0.05$, **: $p \leq 0.01$, ***: $p \leq 0.001$.
764 Color of asterisks corresponds to that of the curve, compared to the single infection.

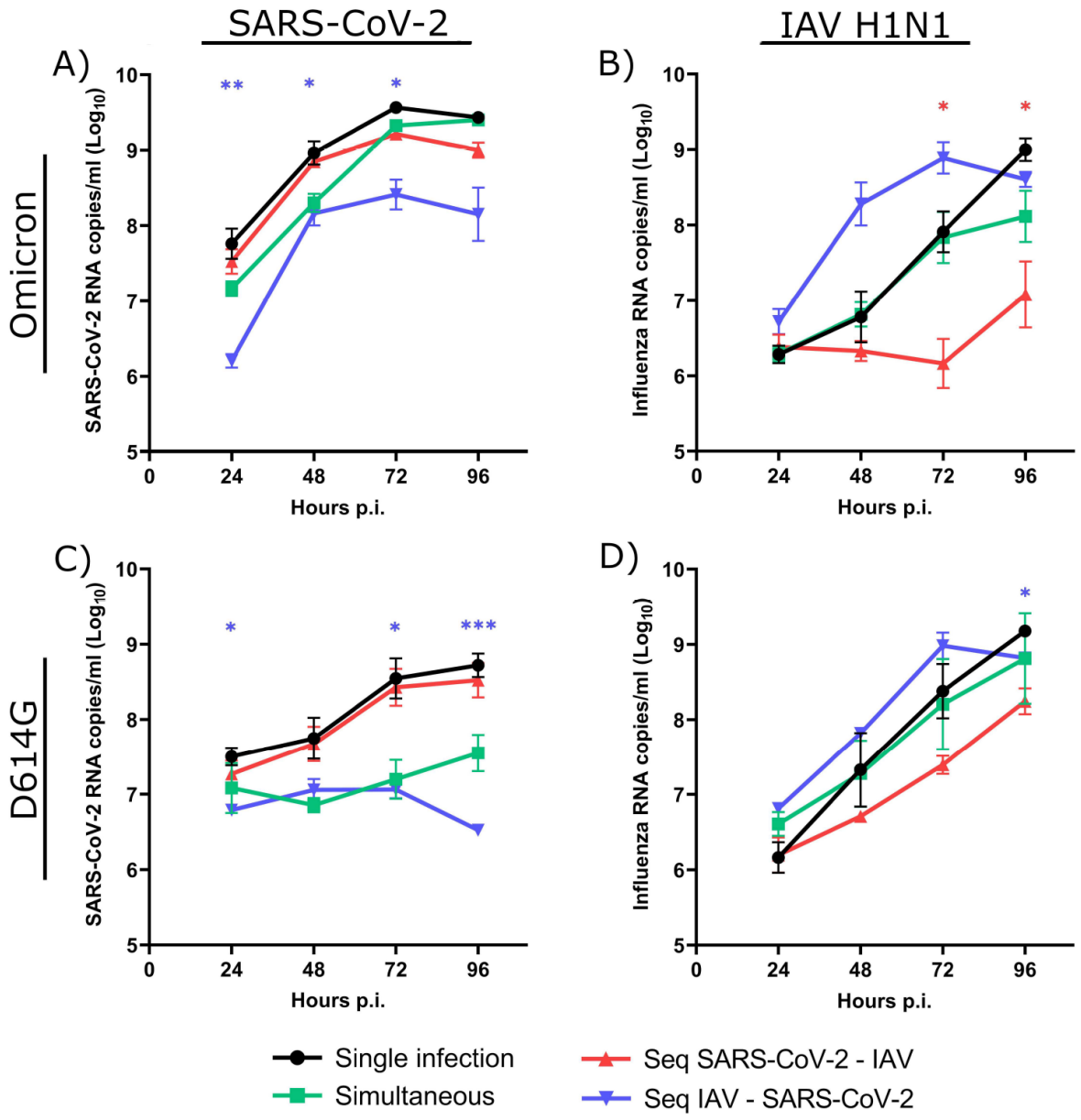

765

766 **Fig 3. Viral interference between SARS-CoV-2 strains and influenza A/H1N1.**

767 Viral RNA loads of SARS-CoV-2 (Omicron variant (A) or D614G mutant (C)) and influenza A/H1N1
768 (B, D) during single infections or simultaneous and sequential (Seq) coinfections in nasal human airway
769 epitheliums (HAEs). Hours post-infection (p.i.) represent the time after the infection with either SARS-
770 CoV-2 (A, C) or influenza (B, D). Results are expressed as the mean of the Log_{10} of viral RNA copies
771 per ml ± SEM of triplicate HAEs in one or two independent experiments. *: $p \leq 0.05$, **: $p \leq 0.01$, ***:
772 $p \leq 0.001$. Color of asterisks corresponds to that of the curve, compared to the single infection.

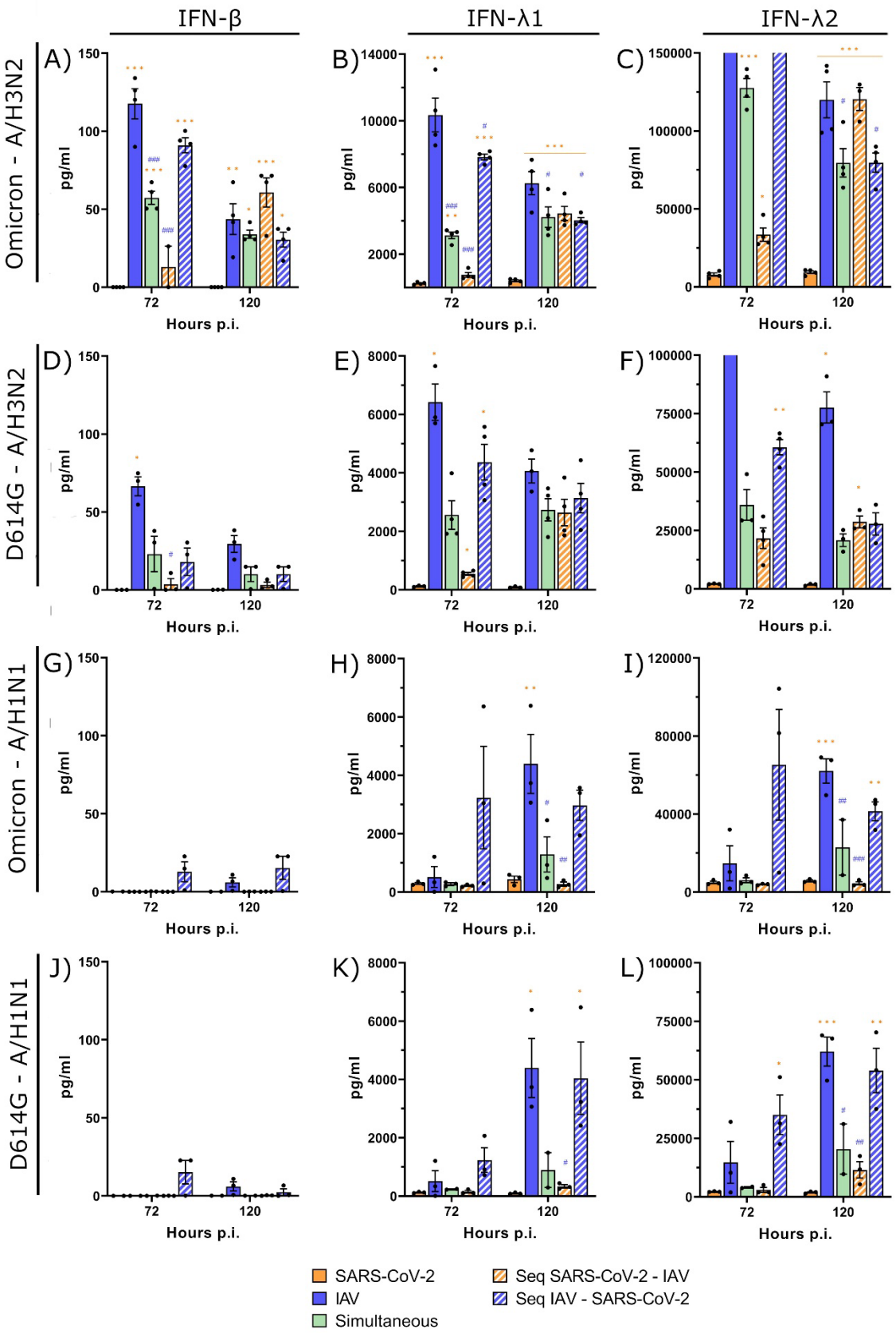
IFN-β
IFN-λ1
IFN-λ2
Omicron - A/H3N2
D614G - A/H3N2
Omicron - A/H1N1
D614G - A/H1N1
A)
B)
C)
D)
E)
F)
G)
H)
I)
J)
K)
L)
pg/ml
Hours p.i.
72
120
SARS-CoV-2
IAV
Simultaneous
Seq SARS-CoV-2 - IAV
Seq IAV - SARS-CoV-2

773

774

775 **Fig 4. Interferon protein production during SARS-CoV-2 and influenza A coinfections.**

776 Type I and type III interferon (IFN-β, IFN-λ1, IFN-λ2) proteins production during single and coinfections
777 of nasal human airway epitheliums with SARS-CoV-2 (Omicron and D614G) and influenza A (H3N2
778 and H1N1) at 72 h and 120 h post-infection (p.i.). Results are expressed as the mean amount of IFN
779 proteins in pg per ml ± SEM of 2 to 6 replicates in one or two independent experiments (bars that appear
780 higher than the Y axis maximum represent values that are "out of range"). Orange *: compared with
781 Omicron alone, blue #: compared with A/H3N2 alone. *, #: $p \leq 0.05$, **, ##: $p \leq 0.01$, ***, ###: $p \leq$
782 0.001.

783

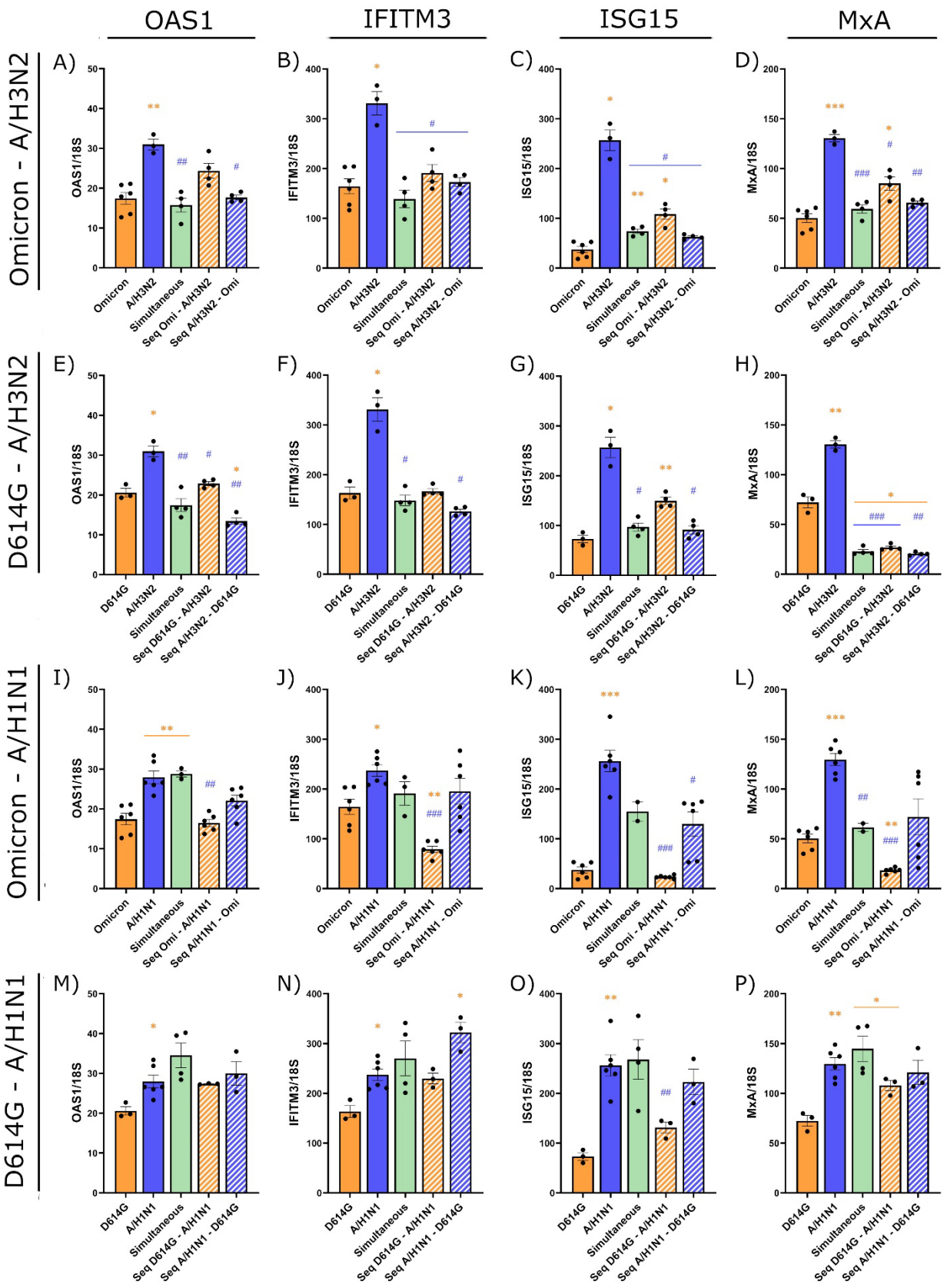
OAS1
IFITM3
ISG15
MxA
Omicron - A/H3N2
D614G - A/H3N2
Omicron - A/H1N1
D614G - A/H1N1
A)
B)
C)
D)
E)
F)
G)
H)
I)
J)
K)
L)
M)
N)
O)
P)
OAS1/18S
IFITM3/18S
ISG15/18S
MxA/18S
Omicron
A/H3N2
Simultaneous
Seq Omi - A/H3N2
Seq A/H3N2 - Omi
D614G
Seq D614G - A/H3N2
Seq A/H3N2 - D614G
A/H1N1
Seq Omi - A/H1N1
Seq A/H1N1 - Omi
Seq D614G - A/H1N1
Seq A/H1N1 - D614G

786 **Fig 5. Interferon-stimulated gene expression during SARS-CoV-2 and influenza A coinfections.**

787 Expression of four interferon-stimulated gene (ISG) mRNAs (OAS1, IFITM3, ISG15, MxA) at 120 h
788 post-infection during single infections or coinfections (simultaneous or sequential (Seq)) with IAV and
789 SARS-CoV-2 strains. Nasal human airway epitheliums were infected with Omicron (Omi) and A/H3N2
790 (panels A-D), D614G and A/H3N2 (panels E-H), Omicron and A/H1N1 (panels I-L), and D614G and
791 A/H1N1 (panels M-P). Results are expressed as the mean of the ratio of ISG mRNAs over that of 18S
792 housekeeping gene (both in copies per µl) ± SEM of 3 to 6 replicates in one or two independent
793 experiments. orange *: compared with Omicron alone, blue #: compared with A/H3N2 alone. *, #: $p \leq$
794 0.05, **, ##: $p \leq 0.01$, ***, ###: $p \leq 0.001$.

795

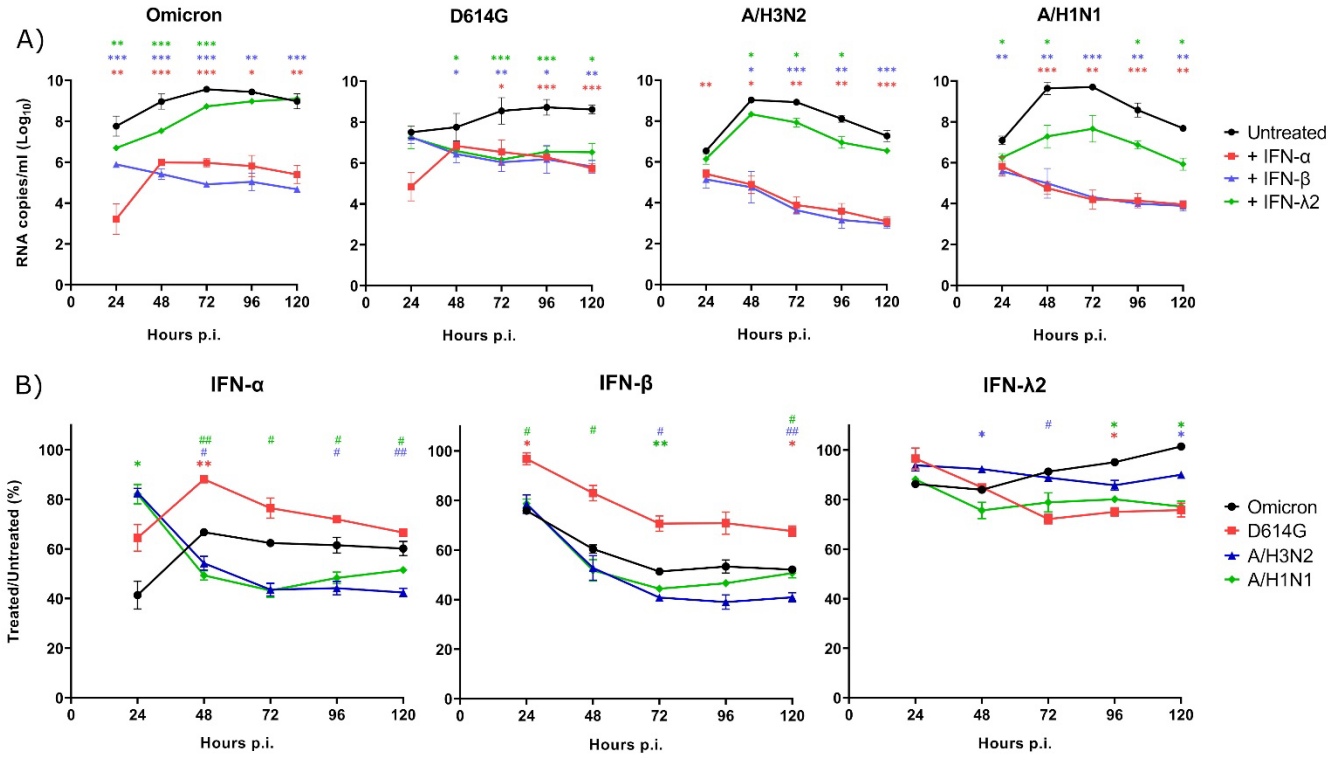

Fig 6. Susceptibility of SARS-CoV-2 and influenza A to recombinant interferon proteins.

A) Viral RNA loads in nasal human airway epitheliums (HAEs) infected with SARS-CoV-2 (Omicron and D614G) and influenza (A/H3N2 and A/H1N1), in presence or absence of recombinant IFN-α2a, IFN-β or IFN-λ2. Results are expressed as the mean of the Log_{10} of viral RNA copies per ml ± SEM of triplicate HAEs in one experiment. A value of 60 copies/ml, corresponding to the detection limit of the assays, was attributed to samples with undetectable RNA levels (n=3). *: $p \leq 0.05$, **: $p \leq 0.01$, ***: $p \leq 0.001$, in comparison with untreated HAEs. B) Comparison of the effects of IFN on the different viruses. Results are expressed as the mean percentage of the viral RNA loads of IFN-treated over untreated HAEs ± SEM using triplicates in one experiment. *: comparison with Omicron, #: comparison with D614G. *, #: $p \leq 0.05$, **, ##: $p \leq 0.01$. Color of symbols corresponds to that of the curve. No significant difference was observed between A/H3N2 and A/H1N1.

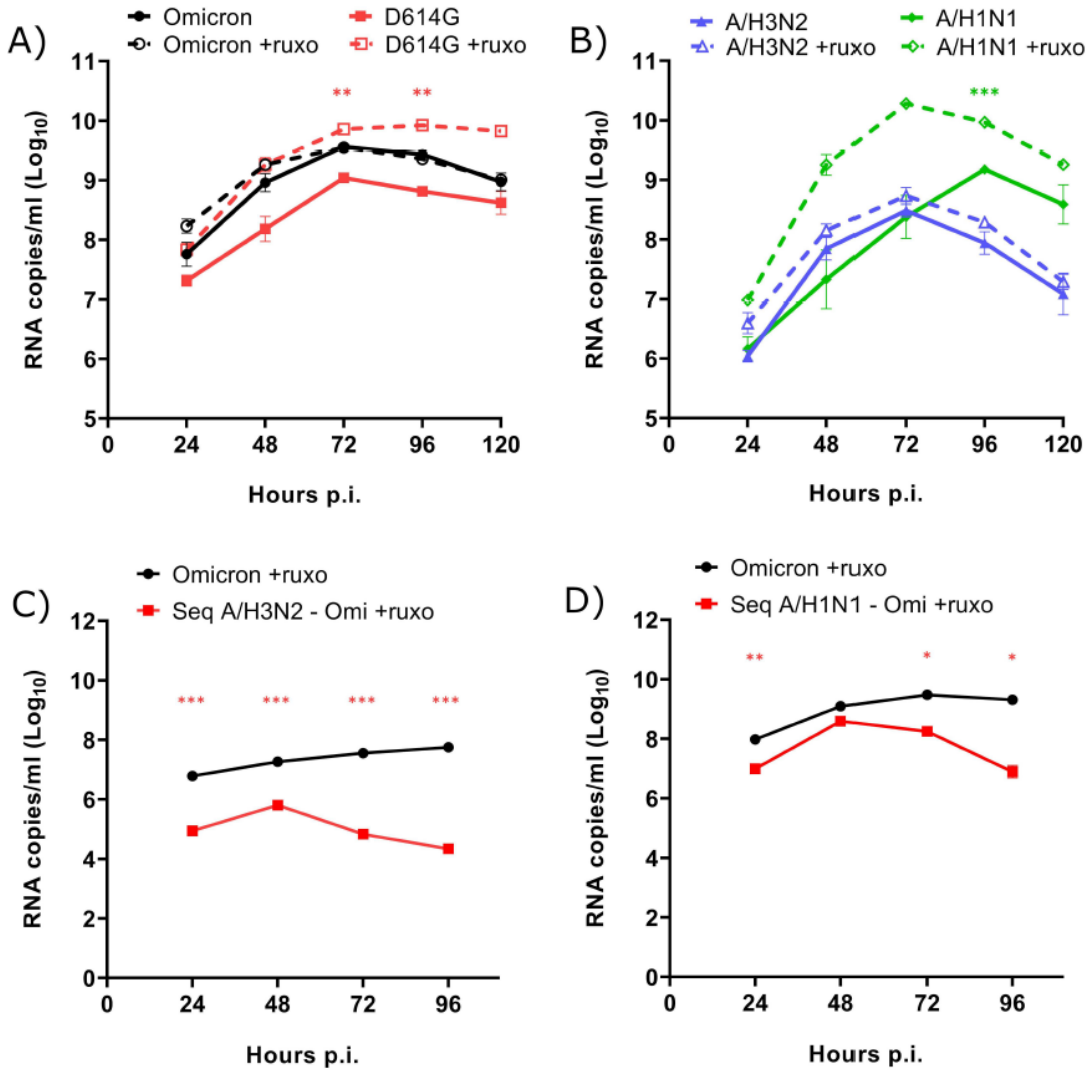

809

810 **Fig 7. Effect of an interferon inhibitor on viral interference between SARS-CoV-2 Omicron and**

811 **influenza A.**

812 Viral RNA loads of A) SARS-CoV-2 (Omicron and D614G) and B) influenza (A/H3N2 and A/H1N1)

813 during single infections in nasal human airway epitheliums (HAEs), in presence or absence of ruxolitinib

814 (ruxo). C-D) Effects of ruxolitinib on viral RNA loads of SARS-CoV-2 Omicron during single infections

815 or sequential (seq) coinfections 24 h after (C) A/H3N2 and (D) A/H1N1. Results are expressed as the

816 mean of the Log_{10} of viral RNA copies per ml ± SEM of 3-4 replicates in one experiment. *: $p \leq 0.05$,

817 **: $p \leq 0.01$, ***: $p \leq 0.001$. Color of asterisks corresponds to that of the curve, compared to untreated

818 HAEs (A, B) or to the single infection (C, D).